

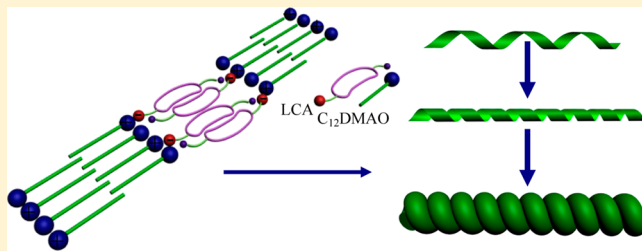
# Room-Temperature Super Hydrogel as Dye Adsorption Agent

Shasha Song, Lei Feng, Aixin Song,\* and Jingcheng Hao

Key Laboratory of Colloid and Interface Chemistry of Ministry of Education, Shandong University, Jinan, 250100, People's Republic of China

## Supporting Information

**ABSTRACT:** Supramolecular hydrogels were prepared in the mixtures of a chiral amphiphilic lithocholic acid (LCA) and a nonionic surfactant, dodecyldimethylamine oxide ( $C_{12}$ DMAO), in water. With the addition of LCA to  $C_{12}$ DMAO micellar solutions, a transition from micelles to gels occurs at room temperature. Hydrogels can form at very low concentrations (below 0.1 wt %), exhibiting a super gelation capability. The rheological measurements show a strong mechanical strength with an elastic modulus exceeding 5000 Pa and a yield stress exceeding 100 Pa. Microstructures determined by TEM, SEM, and AFM observations demonstrate that the gels are formed by intertwined helical fibrils. The formation of fibrils is induced by enormous cycles of units composed of two LCA molecules and four  $C_{12}$ DMAO molecules driven by comprehensive noncovalent interaction, especially the hydrogen bonds produced in two reversed LCA molecules and the  $C_{12}$ DMAOH<sup>+</sup>– $C_{12}$ DMAO pairs. The xerogels show excellent adsorption capability of the toxic dye with a maximum adsorption value of 202 mg·g<sup>-1</sup>.



## INTRODUCTION

Gels are commonplace household materials that have pervaded our everyday life in various kinds of forms such as hair gel, shampoo, toothpaste, and other cosmetics.<sup>1–3</sup> In recent years, gels formed by small organic compounds with molecular masses less than 3000 were termed low molecular weight gels (LMWGs) or supramolecular gels. They have attracted much attention due to their potential applications in drug delivery,<sup>4</sup> tissue engineering, wound healing,<sup>5</sup> cell growth,<sup>6</sup> regenerative medicine,<sup>7</sup> crystal growth,<sup>8–10</sup> reaction media,<sup>11</sup> templating or transcribing self-assembled morphology,<sup>12,13</sup> molecular electronics,<sup>14</sup> and sensing.<sup>15</sup>

Generally, gels are viscoelastic and solidlike materials consisting of an elastic cross-linked network and a solvent, which is the dominant component. The cross-linked networks are formed by the intertwining of fibrils, which are generated by the self-assembled gelators. Among various self-assemblies, helical structures have captivated the interest of scientists over decades because they are associated with many biological events. Helices are the central structural motifs for biological systems, ranging from nanoscopic DNA double helices and collagen triple helices to microscopic viruses and macroscopic seashells. Inspired by the elegance and complexity in nature, great efforts have contributed to constructing helical supramolecular structures with controlled morphology because of their potential applications in materials science and enantioselective catalysis.<sup>16–18</sup> A number of helices have been observed in a variety of systems utilizing chiral “monomers” such as bile salts, amino acids, peptides, and their derivatives.<sup>19–28</sup>

Because gelation is a balance between crystallization and solubilization, amphiphilic molecules with hydrophobic groups

to promote aggregation and hydrophilic groups to provide solubility are most likely to be competent gelators.<sup>29</sup> The biocompatibility of gel materials is crucial for biologically directed applications and environmental considerations.<sup>30</sup> Lithocholic acid (LCA), a biocompatible bile acid, is an end product of the metabolism of cholesterol with several chiral centers and a rigid hydrophobic steroid nucleus.<sup>31,32</sup> Due to the rigid skeleton and the chiral structure of LCA molecules, many supramolecular systems participated in by LCA and its derivatives exhibit novel and abundant self-assembly behaviors, which have been gradually acquired in recent decades. Tubular morphology was observed in the alkaline aqueous solutions of sodium and ammonium salts of LCA.<sup>13,32–34</sup> In addition, hydrogel formation by mixing LCA with individual dimeric or oligomeric amines at specified ratios in water was also observed.<sup>35,36</sup> In the hydrogels, the ion pairs between LCA molecules and dimeric or oligomeric amines lead to the formation of hydrogen bonded networks, which eventually give rise to the formation of hydrogel phase.

For the methods of preparing LMWGs, a cooling process is general to realize the gelation from isotropic solutions at a higher temperature (above the sol–gel temperature,  $T_{\text{gel}}$ ) to gels, which induces the solidification of the self-assembly structures. Comparatively, the formation of supramolecular gels at room temperature has been barely reported except for several results of metallogels and gelations in nonaqueous

Received: July 3, 2012

Revised: September 6, 2012

Published: October 1, 2012



solutions,<sup>37–42</sup> which is the deficiency of the gel family and restricts the applications of the gels.

Herein, we report a supramolecular gel system having super gelation capability and high dye adsorption capability produced by the mixtures of LCA and a nonionic surfactant, dodecyldimethylamine oxide ( $C_{12}$ DMAO), in water. The gels were induced by the chiral spatial interaction and hydrogen bonds, consisting of helical fibrils by modulating the ratios of LCA to  $C_{12}$ DMAO. Compared with general hydrogels, gelation in the studied system was achieved at rather low temperatures (about 10–35 °C) under sufficient mixing of gelators. The dried gel was found to adsorb the dye in wastewater efficiently in an environmentally friendly way.

## EXPERIMENTAL SECTION

**Chemicals and Materials.** Lithocholic acid (LCA, >98%) was purchased from Acros Organics (USA) and used without further purification. Amido black 10B, chrome azurol S, rhodamine 6G, and methyl orange were purchased from Shanghai Chemical Co. (China) and were of p.a. quality.  $C_{12}$ DMAO was purchased from the affiliate of Clariant Co. (Germany) in China and was delivered as 30 wt % aqueous solution. The solutions were freeze-dried and then crystallized three times in acetone. The obtained powders were detected by liquid chromatography–mass spectrometry (Supporting Information, Figure S1 and Table S1) with a purity of 99.2 wt %. Ultrapure water with a resistivity of 18.25 MΩ·cm was obtained using a UPH-IV ultrapure water purifier (China).

**Sample Preparation.** Different amounts of LCA were weighed accurately into test tubes, and then  $C_{12}$ DMAO solutions were added until the final volume of each sample reached 5 mL. The solutions were stirred mildly at room temperature until LCA dissolved completely. Then the samples were equilibrated at 25.0 ± 0.1 °C for at least 4 weeks before the phase behavior was inspected.

**Methods and Characterization.** For field-emission scanning electron microscopy (FE-SEM) observations, a drop of gel solution was placed on a silica wafer to form a thin film. The wafers were freeze-dried in a vacuum extractor at –55 °C and were observed on a Hitachi S4800 FE-SEM at 5.0 kV.

For transmission electron microscopy (TEM) observations, about 4 μL of solution was placed on a TEM grid (copper grid, 3.02 mm, 200 mesh, coated with Formvar film) and the excess solution was wicked away with filter paper. The copper grids were freeze-dried and observed on a JEOL JEM-1400 TEM operating at 120 kV. The images were recorded on a Gatan multiscan CCD and processed with a digital micrograph.

For atomic force microscopy (AFM) observations, a drop of gel solution was placed on a silica wafer, and the excess gel was removed using small forceps to generate thin films on the wafer. The wafers were freeze-dried at –55 °C for 7 days and then were observed using a digital instrument (NanoScope III) operating in tapping mode. An NSC35/AlBS silicon tip with a cantilever length of 90 μm was employed with the resonance frequency region of 240–405 kHz and a scan rate of 1.0 Hz.

Circular dichroism (CD) spectra were obtained using a JASCO J-810 spectropolarimeter, which was flushed with nitrogen during operation. Wavelength scans were recorded at 0.1 nm intervals from 300 to 180 nm. The hydrogels were determined using a 0.1 mm path length quartz cuvette; the micellar solution used a 1 mm path length quartz cuvette.

The rheological measurements were carried out on a HAAKE RS6000 rheometer with a cone–plate system (Ti,

diameter, 35 mm; cone angle, 1°). In oscillatory measurements, an amplitude sweep at a fixed frequency of 1 Hz was performed prior to the following frequency sweep in order to ensure that the selected stress was in the linear viscoelastic region. The viscoelastic properties of the samples were determined by oscillatory measurements in the frequency range 0.01–10 Hz. The samples were measured at 25.0 ± 0.1 °C with the help of a cyclic water bath.

The hydrogels and the  $C_{12}$ DMAO solutions were measured on a VERTEX-70/70v Fourier transform infrared (FT-IR) spectrometer (Bruker Optics, Germany).

The XRD patterns were recorded using a Rigaku D/Max 2200-PC diffractometer with Cu Kα radiation ( $\lambda = 0.154\text{18 nm}$ ) and a graphite monochromator. The samples were measured at room temperature between 1 and 10° in the  $2\theta$  scan mode ( $2.5^\circ \text{ min}^{-1}$ ).

The UV-vis absorption spectra measurements were performed using a HITACHIU-4100 spectrophotometer. The scan rate for each measurement was 200 nm/min.

## RESULTS AND DISCUSSION

**Gelation Behavior.** The formation of hydrogels is directly realized at room temperature without heating. Figure 1 shows

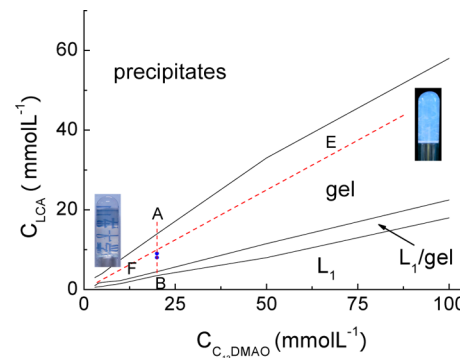


**Figure 1.** Phase diagram of  $C_{12}$ DMAO/LCA system at 25.0 ± 0.1 °C. The inserted photos are gels formed by 2  $\text{mmol}\cdot\text{L}^{-1}$   $C_{12}$ DMAO/1  $\text{mmol}\cdot\text{L}^{-1}$  LCA (left) and 100  $\text{mmol}\cdot\text{L}^{-1}$   $C_{12}$ DMAO/50  $\text{mmol}\cdot\text{L}^{-1}$  LCA (right).

the gel phase region in the  $C_{12}$ DMAO/LCA system. In this work, we focus on the properties of the gel phase, including the gelation ability, the microstructure, and the mechanical strength. The phase boundary is mainly confirmed by visual observations. At a fixed  $C_{12}$ DMAO concentration ( $c_{C_{12}\text{DMAO}}$ ), with the addition of LCA, the  $C_{12}$ DMAO micellar solutions will transform to gels passing a  $L_1/\text{gel}$  two phase, and finally the undissolved LCA forms precipitates. For gels, the gelation capability is quantitatively evaluated by determining the “critical gelator concentration” (CGC),<sup>43</sup> which can be defined as either the minimum amount of gelators required to gelate 1 mL of solvent or the minimum mass fraction of the gelators for the gel formation. In the present system, gels can form at or even lower than 0.1 wt % (the images of the sample can be seen in Figure 1), which is equivalent to the composition of 2  $\text{mmol}\cdot\text{L}^{-1}$   $C_{12}$ DMAO/1  $\text{mmol}\cdot\text{L}^{-1}$  LCA. In other words, at least 54 000 water molecules can be immobilized per unit of LCA molecule with related  $C_{12}$ DMAO molecules, demonstrating the super gelation ability. Gels formed at low concentration (below about 1 wt %) are transparent, while those formed at higher concentration appear opaque, indicating the existence of large

species (the photos inserted in Figure 1). For further study, two series of samples were selected. One was along line AB in Figure 1, with the fixed  $C_{12}\text{DMAO}$  concentration of 20  $\text{mmol}\cdot\text{L}^{-1}$  and different amounts of LCA. Another was along line EF, with the fixed molar ratio of  $C_{12}\text{DMAO}$  to LCA of 2:1 and various total surfactant concentrations.

**Microstructures of the Hydrogels.** Figure 2 shows the microscopic images of hydrogels with different compositions.

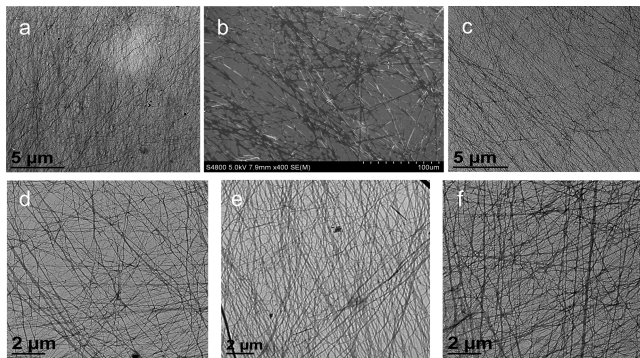


**Figure 2.** TEM (a, c, d, e, and f) and SEM (b) images of freeze-dried gels formed by (a and b) 3  $\text{mmol}\cdot\text{L}^{-1}$   $C_{12}\text{DMAO}$ /1.5  $\text{mmol}\cdot\text{L}^{-1}$  LCA, (c) 5  $\text{mmol}\cdot\text{L}^{-1}$   $C_{12}\text{DMAO}$ /2.5  $\text{mmol}\cdot\text{L}^{-1}$  LCA, (d) 20  $\text{mmol}\cdot\text{L}^{-1}$   $C_{12}\text{DMAO}$ /5  $\text{mmol}\cdot\text{L}^{-1}$  LCA, (e) 20  $\text{mmol}\cdot\text{L}^{-1}$   $C_{12}\text{DMAO}$ /8  $\text{mmol}\cdot\text{L}^{-1}$  LCA, and (f) 20  $\text{mmol}\cdot\text{L}^{-1}$   $C_{12}\text{DMAO}$ /10  $\text{mmol}\cdot\text{L}^{-1}$  LCA.

The three-dimensional network structures are formed through the physical entanglement of one-dimensional fibrils, which immobilize water molecules through solvation and surface tension, resulting in the gelation. The diameters of fibrils formed at the same composition (Figure 2a,b) observed from SEM (about 1  $\mu\text{m}$ ) are much larger than those from TEM (about 200 nm). The difference might be caused by the formation of fibril bundles during the sample preparation for SEM observations. Figure 2a,c shows the fibrils formed at different concentrations with the same molar ratio of  $C_{12}\text{DMAO}$  to LCA of 2:1 (line EF in Figure 1). The diameters of fibrils have no obvious changes. For another series of samples (line AB in Figure 1), similar results can be gained from Figure 2d,e. With detailed observation of Figure 2f, one can find that, with the increase in concentration of gelators, a few bundles of fibrils form with larger diameters due to the increase in fibril density, which might be the reason for the

opacity of the gels at high concentration. Herein, we do not give the electron images of hydrogels at higher concentration because the networks formed by the fibril bundles become more and more dense, and eventually are hardly observed.

The AFM images in Figure 3 provide more information about the microstructures. For the preparation of samples, several problems should be noticed. First, the samples should be in lower concentration in order to avoid the formation of fibril bundles during the freeze-dried process. Second, the hydrogel film generated on the substrates should be thin. Because of the high viscoelasticity, the samples must be dried completely to avoid polluting the probe used in AFM measurements. From Figure 3a a number of long helical fibrils can be observed. The fibrils are about 400 nm in width and about 40 nm in height (Figure 3c). The width of the fibrils obtained from AFM (about 400 nm) is larger than that from TEM (200 nm), which is understandable considering the broadening effect of AFM tips. Figure 3b and Figures S2 and S3 (Supporting Information) show the helical structures clearly with the helical pitch (the distance between two adjacent turns) of about 600 nm (Supporting Information, Figure S2a). Further observation demonstrates that the helical fibrils are formed through a coiling process of the twist ribbons (magnified images in Figure 3c and pointed to by arrows). The thickness of the ribbons was about 0.5 nm (Supporting Information, Figure S2b), just the width of a cholate skeleton.<sup>16</sup>

**Circular Dichroism (CD).** CD spectroscopy is a powerful tool for the characterization of the molecular self-assembly with chirality.<sup>44</sup> The CD spectra of the micellar solution and the hydrogels are shown in Figure 4. No CD signal can be found in the micellar solution (curve 1). With the addition of the LCA, the micellar solution transforms to hydrogels. The hydrogels show a negative band in the wavelength range of 205–260 nm and a positive band in the wavelength range of 181–205 nm (curve 2). Compared with the micellar solution, the remarkable CD signal for the hydrogel proves the formation of an ordered chiral structure, which supports the existence of the helical fibrillar structure.

**Rheological Properties.** The solid network structure of gels, when implanted to be sheared under an increasing stress, will break suddenly at a critical shear stress,  $\tau^*$ , beyond which a Newtonian-like flow occurs.<sup>30</sup> The critical shear stress,  $\tau^*$ , is just the so-called “yield stress”, reflecting the strength of the network structures. Figure 5a shows the shear-induced phase

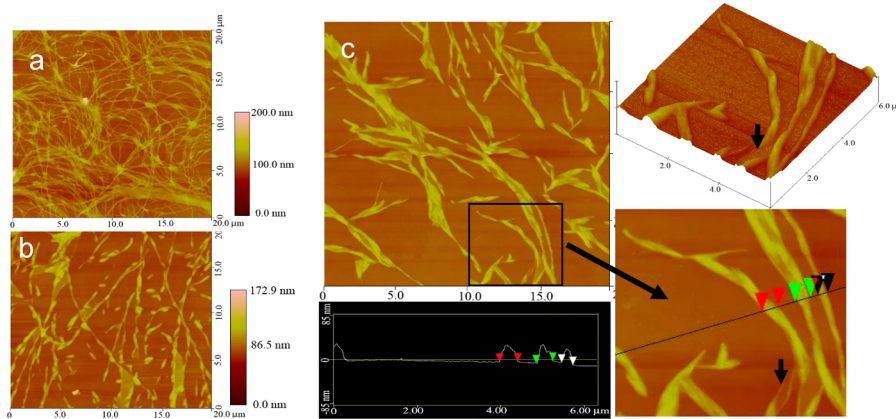


**Figure 3.** AFM images of the hydrogels formed by (a) 3  $\text{mmol}\cdot\text{L}^{-1}$   $C_{12}\text{DMAO}$ /1.5  $\text{mmol}\cdot\text{L}^{-1}$  LCA, (b) 10  $\text{mmol}\cdot\text{L}^{-1}$   $C_{12}\text{DMAO}$ /2.5  $\text{mmol}\cdot\text{L}^{-1}$  LCA, and (c) 20  $\text{mmol}\cdot\text{L}^{-1}$   $C_{12}\text{DMAO}$ /5  $\text{mmol}\cdot\text{L}^{-1}$  LCA.

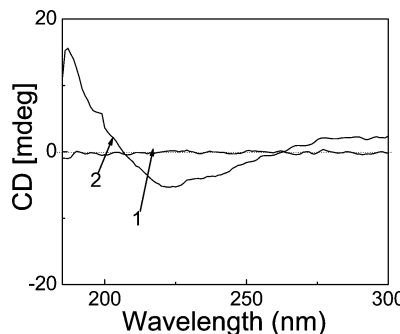


**Figure 4.** CD spectra of samples formed by  $50 \text{ mmol}\cdot\text{L}^{-1}$   $\text{C}_{12}\text{DMAO}/5 \text{ mmol}\cdot\text{L}^{-1}$  LCA system (curve 1, micellar solution) and  $50 \text{ mmol}\cdot\text{L}^{-1}$   $\text{C}_{12}\text{DMAO}/12.5 \text{ mmol}\cdot\text{L}^{-1}$  LCA (curve 2, hydrogel).

transition of samples along line EF in Figure 1. It is found that at a very low concentration,  $3 \text{ mmol}\cdot\text{L}^{-1}$   $\text{C}_{12}\text{DMAO}/1.5 \text{ mmol}\cdot\text{L}^{-1}$  LCA (about 0.15 wt %), the gel has a viscosity value of about  $1000 \text{ Pa}\cdot\text{s}$  and a yield stress value of  $0.8 \text{ Pa}$ , indicating the existence of network structures. With the increase in concentration of gelators, the yield stress increases gradually, ranging from  $0.8$  to  $130 \text{ Pa}$  ( $100 \text{ mmol}\cdot\text{L}^{-1}$   $\text{C}_{12}\text{DMAO}/50 \text{ mmol}\cdot\text{L}^{-1}$  LCA, 5 wt %), which is ascribed to the more rigid network structures induced by increasing fibril density. Simultaneously, the viscosity of the hydrogels also increases. For the sample formed by  $100 \text{ mmol}\cdot\text{L}^{-1}$   $\text{C}_{12}\text{DMAO}/50 \text{ mmol}\cdot\text{L}^{-1}$  LCA (5 wt %), the viscosity even reaches  $10^7 \text{ Pa}\cdot\text{s}$ , demonstrating the characteristic of soft viscoelastic solids.<sup>30,45</sup> Figure 5b shows the rheological properties of four selected samples along line AB in Figure 1. At a fixed  $c_{\text{C}_{12}\text{DMAO}}$  of  $20 \text{ mmol}\cdot\text{L}^{-1}$ , with the increase in LCA concentration from  $8$  to  $10 \text{ mmol}\cdot\text{L}^{-1}$ , the yield stress increases from  $3.2$  to  $25 \text{ Pa}$  and the viscosity increases from  $5000$  to  $10^6 \text{ Pa}\cdot\text{s}$  first. With the further increase in LCA amounts, the yield stress does not change any more, implying the existence of a certain ratio of  $\text{C}_{12}\text{DMAO}$  to LCA to form helical fibrils. Further study proves that the molar ratio of  $\text{C}_{12}\text{DMAO}$  to LCA is  $2:1$ . As reflected by the above results, the hydrogels formed in the  $\text{C}_{12}\text{DMAO}/\text{LCA}$  system exhibit excellent mechanical strength.

The elastic modulus ( $G'$ ) is another important parameter to characterize the strength of gels, from which one can estimate the degree of resistance against mechanical disturbance.<sup>43</sup> During the oscillatory frequency sweep, the stress of  $1 \text{ Pa}$  was chosen (much lower than the yield stress value in the linear viscoelastic region) to be nondestructive to the gel structure. Figure 6 shows the similar rheological behavior of two selected samples. The elastic modulus ( $G'$ ) and viscous modulus ( $G''$ )

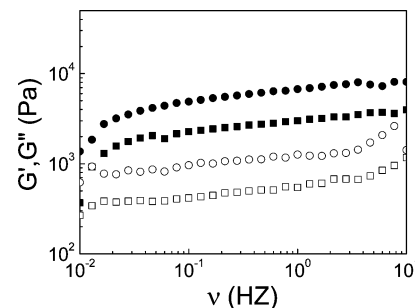


**Figure 6.**  $G'$  (solid symbols) and  $G''$  (open symbols) as a function of oscillatory frequency of hydrogels formed by  $20 \text{ mmol}\cdot\text{L}^{-1}$   $\text{C}_{12}\text{DMAO}/10 \text{ mmol}\cdot\text{L}^{-1}$  LCA (square symbols) and  $50 \text{ mmol}\cdot\text{L}^{-1}$   $\text{C}_{12}\text{DMAO}/25 \text{ mmol}\cdot\text{L}^{-1}$  LCA (round symbols).  $T = 25.0 \pm 0.1 \text{ }^\circ\text{C}$ .

are almost independent of the frequency over the studied frequency region and show an elastic dominant property, demonstrating a solidlike rheological behavior.<sup>30,45</sup> At the concentration of  $1 \text{ wt } \%$  ( $20 \text{ mmol}\cdot\text{L}^{-1}$   $\text{C}_{12}\text{DMAO}/10 \text{ mmol}\cdot\text{L}^{-1}$  LCA),  $G'$  and  $G''$  can reach about  $3000 \text{ Pa}$  and  $300 \text{ Pa}$ , respectively, implying the rigid network structure. With the increase in concentration, the more compact network structure induces the increase of  $G'$  and  $G''$ , reaching about  $5000 \text{ Pa}$  and  $800 \text{ Pa}$ , respectively, at  $2.5 \text{ wt } \%$  ( $50 \text{ mmol}\cdot\text{L}^{-1}$   $\text{C}_{12}\text{DMAO}/25 \text{ mmol}\cdot\text{L}^{-1}$  LCA).

**Discussion.** The proposed mechanism of the formation of different aggregates is shown in Scheme 1. Micelles form in  $\text{C}_{12}\text{DMAO}$  solutions mainly driven by the hydrophobic interaction.<sup>46</sup> When LCA is added, the LCA molecules insert in the monolayer of  $\text{C}_{12}\text{DMAO}$  micelles to form mixed micelles. In the mixtures, the LCA molecules protonate  $\text{C}_{12}\text{DMAO}$  molecules with the carboxyl group to form  $\text{C}_{12}\text{DMAOH}^+ \cdots \text{LC}^-$  ion pairs. Furthermore, besides the electrostatic interaction,  $\text{C}_{12}\text{DMAOH}^+$  also forms hydrogen bonds with nonprotonated  $\text{C}_{12}\text{DMAO}$  molecules ( $\text{C}_{12}\text{DMAOH}^+ \cdots \text{C}_{12}\text{DMAO}$ ), which has been proved by Kawasaki et al. in protonated alkyldimethylamine oxide aqueous solutions.<sup>47,48</sup> With the increase in LCA amounts, the monolayers are not at the stable situation because of the rigid steroidal skeleton of LCA molecules and the hydrophilic hydroxyl groups on the skeleton locating in the hydrophobic cores of the micelles, which induces a transition from micelles to helical fibrils. Based on experimental results, the suggested arrangement in the helical fibrils has been provided. As shown in Scheme 1, besides the electrostatic interaction ( $\text{C}_{12}\text{DMAOH}^+ \cdots \text{LC}^-$ ) and the hydrophobic interaction, there are two kinds of hydrogen bonds existing in the fibril structure.

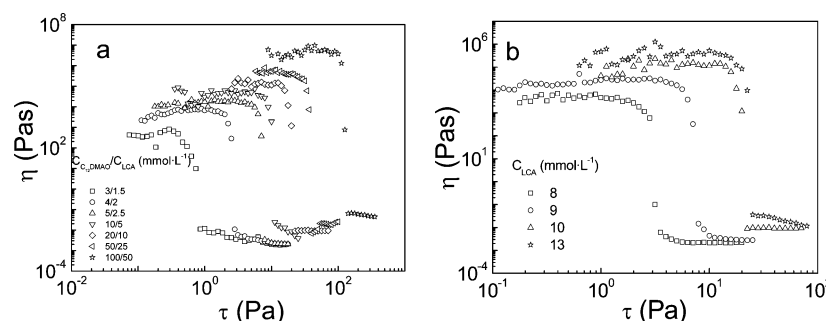
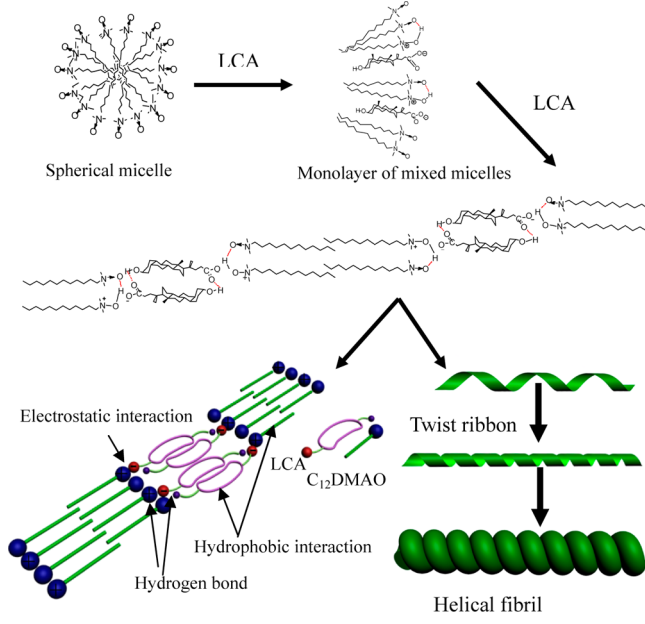


**Figure 5.** Viscosity as a function of shear stress of hydrogels formed (a) at the molar ratio of  $\text{C}_{12}\text{DMAO}$  to LCA of  $2:1$  with different LCA concentrations and (b) at different molar ratios of  $\text{C}_{12}\text{DMAO}$  to LCA at  $c_{\text{C}_{12}\text{DMAO}} = 20 \text{ mmol}\cdot\text{L}^{-1}$ .  $T = 25.0 \pm 0.1 \text{ }^\circ\text{C}$ .

**Scheme 1. Proposed Mechanism of Helical Fibrils Formed in C<sub>12</sub>DMAO/LCA System**



One is between C<sub>12</sub>DMAOH<sup>+</sup> ions and C<sub>12</sub>DMAO molecules, and the other exists between the carboxyl groups of LCA molecules and the hydroxyl groups of other reversed LCA molecules. Combined with hydrophobic interaction, the fibrils are constructed by arrays arranged by enormous cycles of units formed by two connected LCA molecules and four C<sub>12</sub>DMAO molecules. The arrays combine with each other through the hydrophobic and van der Waals interactions to form ribbons, exhibiting a thickness the width of an LCA molecule. Due to the rigid steroid skeleton and chiral structure of the LCA molecule, the arrays cannot extend in linearity, but tilt to induce the formation of helical fibrils coiled by ribbons.

The element analysis and FT-IR and X-ray diffraction (XRD) experiments were performed to support the proposed mechanism of the formation of the fibrils in hydrogels. When the network structure is destroyed by violent shaking, the fibrils separate from solvents and combine to thick bundles, suspending in solutions. The suspended bundles can be taken from the solutions and characterized by optical microscopy (Supporting Information, Figure S4) and element analysis (Supporting Information, Table S2), from which we conclude that the helical fibrils are formed by C<sub>12</sub>DMAO combined with LCA with a constant molar ratio of 2:1.

FT-IR spectroscopy is powerful enough to detect the hydrogen bond, which usually exhibits intense and continuous absorption peaks within the region of 1600–400 cm<sup>-1</sup> in FT-IR spectra.<sup>48–52</sup> Due to the formation of the hydrogen bonds, the stretching vibration of the relevant atom usually shows a bathochromic shift and the bending vibration shows a hypsochromic shift. For C<sub>12</sub>DMAO micellar solution in Figure 7a, the stretching vibration of C–N–O and the bending vibration of –CH<sub>2</sub>– at about 1330 cm<sup>-1</sup> (labeled as peak A) are very weak. When HCl is added, part of C<sub>12</sub>DMAO molecules are protonated to be C<sub>12</sub>DMAOH<sup>+</sup>, and then the strong hydrogen bond forms between C<sub>12</sub>DMAOH<sup>+</sup> and C<sub>12</sub>DMAO. Correspondingly, peak A is enhanced (curve b in Figure 7). The bending vibration of the C–N–O group at 1196 cm<sup>-1</sup> (labeled as peak B) is also enhanced and shifts to about

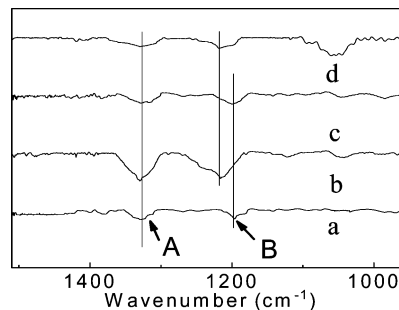


**Figure 7.** FT-IR spectra of samples formed by 100 mmol·L<sup>-1</sup> C<sub>12</sub>DMAO with (a) 0, (b) 50, and (c) 100 mmol·L<sup>-1</sup> HCl. Curve d is the spectrum of the gel formed by 100 mmol·L<sup>-1</sup> C<sub>12</sub>DMAO with 50 mmol·L<sup>-1</sup> LCA.

1216 cm<sup>-1</sup>. When the HCl amount is equal to or greater than that of C<sub>12</sub>DMAO, C<sub>12</sub>DMAO molecules are totally protonated and the hydrogen bonds cannot form. Therefore, the bending vibration of C–N–O does not show any shift (curve c in Figure 7). For hydrogels formed in the C<sub>12</sub>DMAO/LCA system, the absorption peak at about 1330 cm<sup>-1</sup> was enhanced and the bending vibration of C–N–O at 1196 cm<sup>-1</sup> shifts to about 1218 cm<sup>-1</sup> (curve d in Figure 7), which implies the formation of hydrogen bonds. The hypsochromic shift is ascribed to the prohibition of the bending vibration of the C–N–O group because of the hydrogen bonding.<sup>53</sup> For the hydrogen bonds between the carboxyl group of the LCA molecule and the hydroxyl group of another reversed LCA molecule, we cannot see clearly in FT-IR spectra due to the weak interaction. Mezzenga<sup>54</sup> has proved the existence of the hydrogen bond between the two LCA molecules.

More information on the fibril structures is revealed by small-angle X-ray diffraction (XRD) patterns, as shown in Figure 8.

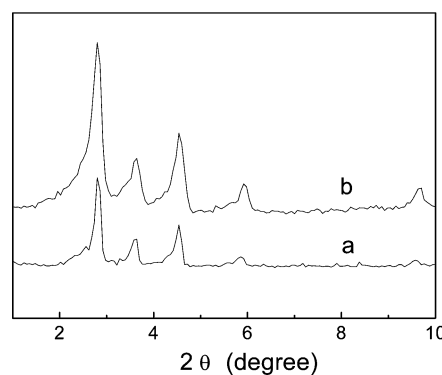


**Figure 8.** Small-angle XRD patterns of dried hydrogels formed by (a) 3 mmol·L<sup>-1</sup> C<sub>12</sub>DMAO/1.5 mmol·L<sup>-1</sup> LCA and (b) 20 mmol·L<sup>-1</sup> C<sub>12</sub>DMAO/9 mmol·L<sup>-1</sup> LCA.

According to Bragg's law, the three well-resolved reflection peaks at 2.8, 3.6, and 4.5° are calculated corresponding to the *d* spacing of 3.15, 2.45, and 1.96 nm, respectively. The *d* value of 3.15 nm is just a little less than twice as long as the chain length of the C<sub>12</sub>DMAO molecule,<sup>55</sup> belonging to the combination of two C<sub>12</sub>DMAO molecules through hydrophobic interaction in each unit of the arrays. The *d* value of 1.96 nm is a little longer than a cholate backbone length (1.5 nm), which might be ascribed to the elongation induced by the connection of two LCA molecules in each unit. For the spacing of *d* = 2.45 nm and other reflection peaks, it is difficult to point out the

accurate belongings. We consider that the reflections are probably related to some cycled units induced by the tilted arrangements.

**Dye Adsorption.** The pH responsive hydrogels and metallohydrogels have been used to adsorb different types of toxic dyes with the intention to purify dye contaminated wastewater.<sup>56–58</sup> In this paper, for a typical process, 0.0384 g of xerogel was submerged in 10 mL of solution containing 7.83 mg of amido black 10B and then left undisturbed. The dye molecules were efficiently entrapped to the xerogels within several hours and the bluish-black solution became crystal clear, as shown in Figure 9. UV-visible spectroscopy was employed

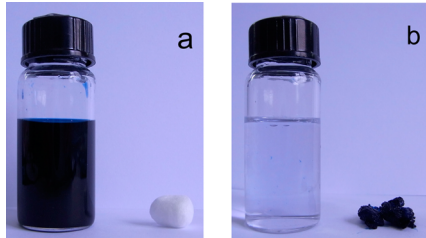


**Figure 9.** Dye solution and dried gels (a) before and (b) after adsorption.

to monitor the adsorption of dye during 24 h with various time intervals (Figure 10). The dye concentration decreases sharply after the addition of xerogels initially, and then decreases gradually, reaching an unchangeable value after 15 h (Figure 10a). Combined with the calibration curve of amido black 10B solutions (Supporting Information, Figure S5), we can conclude from Figure 9b that almost all the dye content can be adsorbed within 15 h with a dye adsorption value of  $202 \text{ mg g}^{-1}$ , which is an excellent result among the reports of supramolecular gels.<sup>56–58</sup> The TEM image in Figure 11 shows that the dye particles are adsorbed on the helical fibril bundles of the xerogels. It is worthwhile to point out that the provided method is green and simple. Because no additive is added in the gelation process, the pollution of water by the introduction of heavy metals, acids, and alkalis during the adsorption process is prohibited.

The adsorption of chrome azurol S, rhodamine 6G, and methyl orange by the xerogels was also studied. The structures of the dye molecules are shown in Figure S7 in the Supporting Information. From the UV-vis spectra (Supporting Information, Figure S6), it is found that the adsorption efficiency is

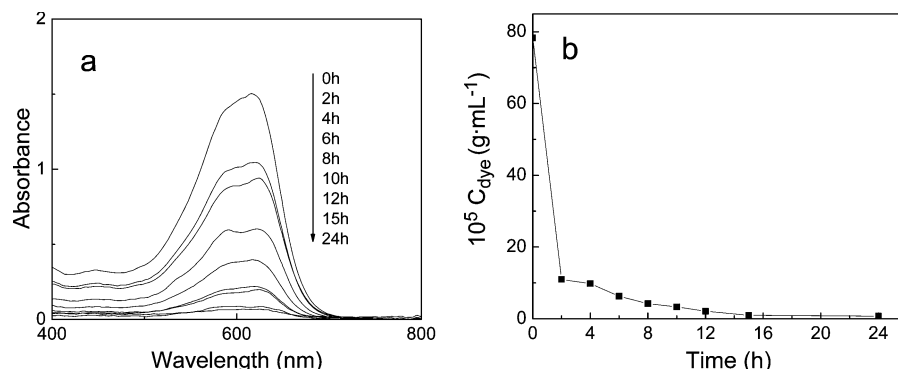


**Figure 10.** UV-vis spectra of (a) dye solution with time after the addition of the xerogels and (b) dye concentration as a function of time. The solution at 0 h was diluted 10 times and others were diluted 2 times before determination.

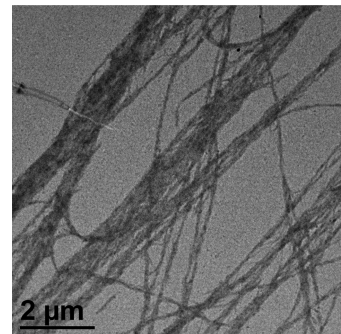


**Figure 11.** TEM image of xerogels after the dye adsorption process.

much lower than that of amido black 10B. FT-IR experiments were carried out in order to detect the reason for the adsorption of amido black 10B. The results (Supporting Information, Figure S8) show that there is no obvious change for the stretching and bending vibration of the  $-\text{NH}_2$  group in amido black 10B, which does not support our assumption that the hydrogen bonding between the carboxyl or hydroxyl in the hydrogels and the  $-\text{NH}_2$  group in amido black 10B is the main determining factor in the adsorption process. Thus, the possible reason could be attributed to the hydrophobic/hydrophilic balance of the dye molecules. Generally, the dye absorbing agents should include two domains: hydrophilic domain to interact with water and hydrophobic domain to adsorb the dye. The hydrophobic/hydrophilic balance of the dye molecule plays an important role in the adsorption process.<sup>58,59</sup> Compared with methyl orange, chrome azurol S, and rhodamine 6G, the highest adsorption efficiency of amido black 10B might be ascribed to the appropriate hydrophobic interaction between the fibrils and the dye molecules.

## CONCLUSION

The supramolecular hydrogels with excellent gelation capability and mechanical strength are realized in aqueous solutions of  $\text{C}_{12}\text{DMAO}$  and LCA at room temperature. The hydrogels are composed of network structures formed by intertwined helical fibrils with a certain composition. A coiling process of twisted ribbons is observed in the formation of helical fibrils. In the present system, the formation of the fibrils was driven by the balance of various interactions, i.e., the electrostatic interaction, the hydrogen bond, the spatial effect induced by the rigid chiral structure, hydrophobic interaction, and van der Waals force. Among them, the multiple hydrogen bonds, two formed

between the two reversed LCA molecules and the other between  $C_{12}\text{DMAOH}^+$  and  $C_{12}\text{DMAO}$ , play an important role in the gelation process. The bile acids are very important in physiological processes and, moreover, are excellent gelators in the preparation of supramolecular hydrogels and correlative material. Moreover, due to the efficient adsorption of the toxic dye molecules, this hydrogel system can be used as an environmentally friendly water-purifying agent. We hope our results will provide useful information in applications in biological and materials science areas.

## ■ ASSOCIATED CONTENT

### Supporting Information

Liquid chromatography–mass spectrometry, AFM images, optical microscope images, elemental analysis, UV–vis spectra, and dye molecular structures. This material is available free of charge via the Internet at <http://pubs.acs.org>.

## ■ AUTHOR INFORMATION

### Corresponding Author

\*E-mail: songaixin@sdu.edu.cn. Tel.: +86-531-88363532.

### Notes

The authors declare no competing financial interest.

## ■ ACKNOWLEDGMENTS

This work is financially supported by the NSFC (Nos. 20833010 and 21173132) and NSF of Shandong Province (ZR2010BM015).

## ■ REFERENCES

- (1) Steed, J. *Chem. Commun.* **2011**, 47, 1379–1383.
- (2) Sangeetha, N.; Maitra, U. *Chem. Soc. Rev.* **2005**, 34, 821–836.
- (3) Piepenbrock, M.; Lloyd, G.; Clarke, N.; Steed, J. *Chem. Rev.* **2010**, 110, 1960–2004.
- (4) Yang, Z.; Liang, G.; Guo, Z.; Guo, Zh.; Xu, B. *Angew. Chem., Int. Ed.* **2007**, 46, 8216–8219.
- (5) Yang, Z.; Xu, K.; Wang, L.; Gu, H.; Wei, H.; Zhang, M.; Xu, B. *Chem. Commun.* **2005**, 4414–4416.
- (6) Mohmeyer, N.; Wang, P.; Schmidt, H.; Zakeeruddin, S.; Gratzel, M. *J. Mater. Chem.* **2004**, 14, 1905–1909.
- (7) Hirst, A.; Escuder, B.; Miravet, J.; Smith, D. *Angew. Chem., Int. Ed.* **2008**, 47, 8002–8018.
- (8) Foster, J.; Piepenbrock, M.; Lloyd, G.; Clarke, N.; Howard, J.; Steed, J. *Nat. Chem.* **2010**, 2, 1037–1043.
- (9) Ilusar, M.; Sanchez, C. *Chem. Mater.* **2008**, 20, 782–820.
- (10) Simon, F.; Khelfallah, N.; Schmutz, M.; Diaz, N.; Mesini, P. *J. Am. Chem. Soc.* **2007**, 129, 3788–3789.
- (11) Escuder, B.; Rodríguez-Llansola, F.; Miravet, J. *New J. Chem.* **2010**, 34, 1044–1054.
- (12) Vemula, P.; John, G. *Chem. Commun.* **2006**, 2218–2220.
- (13) Terech, P.; Sangeetha, N.; Bhat, S.; Allegraud, J.; Buhler, E. *Soft Matter* **2006**, 2, 517–522.
- (14) Puigmartí-Luis, J.; Laukhin, V.; Pérez del Pino, Á.; Vidal-Gancedo, J.; Rovira, C.; Laukhina, E.; Amabilino, D. *Angew. Chem., Int. Ed.* **2007**, 46, 238–241.
- (15) Yang, Z.; Ho, P.; Liang, G.; Chow, K.; Wang, Q.; Cao, Y.; Guo, Z.; Xu, B. *J. Am. Chem. Soc.* **2007**, 129, 266–267.
- (16) Qiao, Y.; Lin, Y.; Wang, Y.; Yang, Z.; Liu, J.; Zhou, J.; Yan, Y.; Huang, J. *Nano Lett.* **2009**, 9, 4500–4504.
- (17) Li, L.; Jiang, J.; Messmore, B.; Bull, S.; Stupp, S. *Angew. Chem., Int. Ed.* **2007**, 46, 5873–5876.
- (18) Yang, Y.; Suzuki, M.; Owa, S.; Shirai, H.; Hanabusa, K. *Chem. Commun.* **2005**, 4462–4464.
- (19) Rogalska, E.; Rogalski, M.; Gulik-Krzywicki, T.; Gulik, A.; Chipot, C. *Proc. Natl. Acad. Sci. U.S.A.* **1999**, 96, 6577–6580.
- (20) Castelletto, V.; Hamley, I.; Hule, R.; Pochan, D. *Angew. Chem., Int. Ed.* **2009**, 48, 2317–2320.
- (21) Pashuck, E.; Stupp, S. *J. Am. Chem. Soc.* **2010**, 132, 8819–8821.
- (22) Tellini, V.; Jover, A.; Meijide, F.; Tato, J.; Galantini, L.; Pavel, N. *Adv. Mater.* **2007**, 19, 1752–1756.
- (23) Tsai, W.; Li, L.; Cui, H.; Jiang, H.; Stupp, S. *Tetrahedron* **2008**, 64, 8504–8514.
- (24) Manghisi, N.; Leggio, C.; Jover, A.; Meijide, F.; Pavel, N.; Tellini, V.; Tato, J.; Agostino, R.; Galantini, L. *Angew. Chem., Int. Ed.* **2010**, 49, 6604–6607.
- (25) Yan, X.; Cui, Y.; Qi, W.; Su, Y.; Yang, Y.; He, Q.; Li, J. *Small* **2008**, 4, 1687–1693.
- (26) Zhu, P.; Yan, X.; Su, Y.; Yang, Y.; Li, J. *Chem.—Eur. J.* **2010**, 16, 3176–3183.
- (27) Yan, X.; Zhu, P.; Li, J. *Chem. Soc. Rev.* **2010**, 39, 1877–1890.
- (28) Yan, X.; Cui, Y.; He, Q.; Wang, K.; Li, J. *Chem. Mater.* **2008**, 20, 1522–1526.
- (29) Estroff, L.; Hamilton, A. *Chem. Rev.* **2004**, 104, 1201–1217.
- (30) Terech, P.; Dourdain, S.; Maitra, U.; Bhat, S. *J. Phys. Chem. B* **2009**, 113, 4619–4630.
- (31) Terech, P.; Geyer, A.; Struth, B.; Talmon, Y. *Adv. Mater.* **2002**, 14, 495–498.
- (32) Zhang, X.; Zou, J.; Tamhane, K.; Kobzeff, F.; Fang, J. *Small* **2010**, 6, 217–220.
- (33) Jean, B.; Oss-Ronen, L.; Terech, P.; Talmon, Y. *Adv. Mater.* **2005**, 17, 728–731.
- (34) Terech, P.; Jean, B.; Ne, F. *Adv. Mater.* **2006**, 18, 1571–1574.
- (35) Pal, A.; Basit, H.; Sen, S.; Aswal, V.; Bhattacharya, S. *J. Mater. Chem.* **2009**, 19, 4325–4334.
- (36) Dastidar, P.; Okabe, S.; Nakano, K.; Iida, K.; Miyata, M.; Tohnai, N.; Shibayama, M. *Chem. Mater.* **2005**, 17, 741–748.
- (37) Cravotto, G.; Cintas, P. *Chem. Soc. Rev.* **2009**, 38, 2684–2697.
- (38) Naota, T.; Koori, H. *J. Am. Chem. Soc.* **2005**, 127, 9324–9325.
- (39) Piepenbrock, M.; Clarke, N.; Steed, J. *Soft Matter* **2010**, 6, 3541–3547.
- (40) Kuang, Y.; Gao, Y.; Shi, J.; Lin, H.; Xu, B. *Chem. Commun.* **2011**, 47, 8772–8774.
- (41) Chen, J.; McNeil, A. *J. Am. Chem. Soc.* **2008**, 130, 16496–16497.
- (42) Lortie, F.; Boileau, S.; Bouteiller, L.; Chassenieux, C.; Ducouret, G.; Jalabert, M.; Terech, P. *Langmuir* **2002**, 18, 7218–7222.
- (43) Ghosh, A.; Dey, J. *Langmuir* **2009**, 25, 8466–8472.
- (44) Wang, T.; Jiang, J.; Liu, Y.; Li, Zh.; Liu, M. *Langmuir* **2010**, 26, 18694–18700.
- (45) Jiang, L.; Yan, Y.; Huang, J. *Soft Matter* **2011**, 7, 10417–10423.
- (46) Fukada, K.; Kawasaki, M.; Kato, T.; Maeda, H. *Langmuir* **2000**, 16, 2495–2501.
- (47) Maeda, H.; Kakehashi, R. *Adv. Colloid Interface. Sci.* **2000**, 88, 275–293.
- (48) Kawasaki, H.; Maeda, H. *Langmuir* **2001**, 17, 2278–2281.
- (49) Wasicki, J.; Jaskolski, M.; Pajak, Z.; Szafran, M.; Dega-Szafran, Z.; Adams, M.; Parker, S. *J. Mol. Struct.* **1999**, 476, 81–95.
- (50) Szafran, M.; Tykarska, E.; Dega-Szafran, Z. *J. Mol. Struct.* **1997**, 416, 81–90.
- (51) Bohner, U.; Zundel, G. *J. Phys. Chem.* **1986**, 90, 964–973.
- (52) Rathman, J.; Scheuing, D. *ACS Symp. Ser.* **1990**, 447, 123–142.
- (53) Song, S.; Zheng, Q.; Song, A.; Hao, J. *Langmuir* **2012**, 28, 219–226.
- (54) Schefer, L.; Sánchez-Ferrer, A.; Adamik, J.; Mezzenga, R. *Langmuir* **2012**, 28, 5999–6005.
- (55) Regev, O.; Guillemet, F. *Langmuir* **1999**, 15, 4357–4364.
- (56) Ray, S.; Das, A.; Banerjee, A. *Chem. Mater.* **2007**, 19, 1633–1639.
- (57) Samai, S.; Biradha, K. *Chem. Mater.* **2012**, 24, 1165–1173.
- (58) Basak, S.; Nanda, J.; Banerjee, A. *Soft Matter* **2009**, 5, 3452–3460.
- (59) Bekiari, V.; Lianos, P. *Chem. Mater.* **2006**, 18, 4142–4146.